Journal of Sound and Vibration 326 (2009) 367–382

Contents lists available at ScienceDirect

Journal of Sound and Vibration

journal homepage: www.elsevier.com/locate/jsvi

Identification of beat characteristics and damping ratios of bell type structures using wavelet transform

Sung Yong Park [a], Yeon June Kang [a,*], Seock Hyun Kim [b]

[a] Advanced Automotive Research Center, School of Mechanical and Aerospace Engineering, Seoul National University, Gwanangno 599, Gwanak-Gu, Seoul 151-744, Republic of Korea

[b] Division of Mechanical and Mechatronics Engineering, Kangwon National University, Hyoja2-Dong 192-1, Chunchon-Si, Kangwon-Do 200-701, Republic of Korea

ARTICLE INFO

Article history:
Received 1 September 2008
Received in revised form
17 February 2009
Accepted 18 April 2009
Handling Editor: L.G. Tham
Available online 2 June 2009

ABSTRACT

The aim of this paper is to propose an effective method for extracting the beat characteristics and modal damping ratios of the bell type structures using the continuous wavelet transform (CWT). The bell type structures which can be simplified as a slightly asymmetric circular ring and cylindrical shell are commonly used to analyze those of a Korean bell. The beat response is caused by the mutual interference of mode pairs, which are created by the slight asymmetry of the bell type structures in the circumferential direction. First of all, the beat frequencies and periods of each vibration mode are obtained using the CWT based on the Gabor wavelet. Next, the modal damping ratios associated with the time duration of the beat response are also extracted by the CWT. When using the CWT on a given signal, the optimal shape of the Gabor wavelet used as the mother wavelet is determined by employing the Shannon entropy cost function on the normalized wavelet modulus. In order to show the accuracy of the proposed method, the beat characteristics and damping ratios are extracted from the simulated pure and noisy signals, which have mode pairs. Finally, the proposed method is applied to a small-sized Korean bell to verify its applicability in the field.

1. Introduction

There are many traditional bells that are designated as national treasures in Korea. They are the Sangwon temple bell (AD 725), the King Seong-deok Divine bell (AD 771) [1], the Yongju temple bell (AD 854), the Cheonheung temple bell (AD 1010), the Bosingak bell (AD 1468) [2] and so on. Many of these Korean bells have two principal characteristics in vibration and sound. First of all, a Korean bell has the beat characteristics, which are caused by the mutual interference of mode pairs that are created by the slight asymmetry of the bell in the circumferential direction. A clear beat and proper beat period are important for the liveliness of the Korean bell sound, while warble or beating sound should be eliminated within the limits of the possible in the western bell [3,4]. Second, a Korean bell has long time duration of the beat in its vibration and sound. The time duration of a beat phenomenon depends on the modal damping ratio associated with the bell material and the cooling speed during its casting. The sonority of the sound in the bell is determined by the relationships among frequencies, intensities, and the decay times of partials. At the instant of impact, most dominant sound qualities are produced by several partial tones. However, higher mode tones decay rapidly after striking and people

* Corresponding author. Tel.: +82 2 880 1691; fax: +82 2 888 5950.
E-mail address: yeonjune@snu.ac.kr (Y.J. Kang).

0022-460X/$ - see front matter © 2009 Elsevier Ltd. All rights reserved.
doi:10.1016/j.jsv.2009.04.039

hear just the sound produced by the first mode (hum tone) and the second mode (fundamental tone), which lasts long. Usually, a long lasting hum or fundamental tone is desired in a Korean bell.

Until now, the theoretical studies on the dynamic characteristics of the bell type structures have been carried out by several researchers. Kim et al. [5] analyzed the beat response of the ring-stiffened shell with an attached concentrated mass using the receptance method. Lee et al. [2] introduced numerical and experimental methods to predict and tune the vibration and sound properties of a large sized Korean bell. Rossing and Perrier [6] studied the vibrational modes of a small Korean bell by using holographic interferometry and modal analysis with impact excitation. Hong and Lee [7] analyzed the mode pairs of a circular ring with a single deviation in the mass and stiffness. Park et al. [8] proposed an analytical method to control the period and the clarity of the beat in a slightly asymmetric ring. They [9] also investigated the effect of multiple local deviations on the property of mode pair in a circular ring. However, much of the previous research has been focused on the theoretical beat characteristics of a bell type structure, such as a circular ring and a cylinder with a point mass and local stiffness.

Up to now, hardly has any experimental research been carried out for identifying the beat characteristics and time duration of the bell type structures. In this paper, the beat characteristics and modal damping ratios of a Korean bell are experimentally identified from the CWT of a measured impulse signal. There are several time-frequency representation tools, such as the CWT, the short time Fourier transform (STFT) and the Wigner–Ville distribution (WVD). In general, the STFT has some limitations in analyzing a signal that varies with an instantaneous frequency because its time-frequency resolution is fixed. The WVD has a better time-frequency resolution than the STFT, but despite its remarkable properties, the WVD has limited applications because it contains the cross-talk effects. The CWT can overcome the limitations of the STFT and the WVD because the time-frequency resolution of the CWT can be controlled adaptively. Recently, several studies have been carried out using the CWT to identify the dynamic properties, which are the modal damping ratio, the natural frequency and the mode shape [10–13]. The wavelet transforms have also used to detect the fault of the mechanical and electric system [14–16]. When the CWT is applied to a measured signal, a systematic method has been studied that will minimize the edge effect of the CWT [17,18].

The aim of this paper is to propose an effective method for extracting the beat characteristics and modal damping ratios of the Korean bell using the CWT analysis. In conventional Fourier transform analysis, the frequency resolution is very critical to effectively separate the given signal into each mode and to exactly extract the modal parameters. In this case, it has an inevitable weakness of increase of the gathering time for an experimental signal. In conventional wavelet analysis, it is also very difficult to decouple the very close two modes such as the beating mode of the Korean bell into each mode due to the proximity of beating frequency. However, the inevitable weakness of the Fourier transform and the limitation of the conventional wavelet transform could be overcome through the simultaneous manipulation of the very close two modes in analyzing the given signal using the continuous wavelet transform. When applying the CWT to the beating response of the Korean bell, the simultaneous manipulation of the low and high mode related with the beating response is carried out without the individual decomposition of two modes.

This paper is organized in the following way. In Section 2, the theoretical background of the CWT is briefly explained. In Section 3, the Shannon entropy cost function used to determine the optimal shape of the mother wavelet is also presented. In Section 4, the mode decoupling process of the multi-degree of freedom system is explained using the CWT. After that, the analytical beat characteristics of each mode are examined using a slightly asymmetric cylindrical shell, which can analyze the beat characteristics of the Korean bell. Next, the beat characteristics and modal damping ratios from the impulse responses of a slightly asymmetric cylindrical are analytically identified using the CWT. Finally, we experimentally verify the proposed method with a small-sized Korean bell.

2. Theoretical background of the continuous wavelet transform

The continuous wavelet transform $W_\psi x(u,s)$ [19] of an L_2-based signal $x(t)$ is defined as

$$W_\psi x(u,s) = \int_{-\infty}^{\infty} x(t)\psi^*_{u,s}(t)\,\mathrm{d}t \tag{1}$$

where

$$\psi_{u,s}(t) = \frac{1}{\sqrt{s}}\psi\left(\frac{t-u}{s}\right), \quad s>0, \ \ u \in R. \tag{2}$$

Here, $\psi^*(t)$ is the complex conjugate of the mother wavelet $\psi(t)$, which is dilated with a scale parameter s related to the frequency and translated by translation parameter u localizing the wavelet in the time-domain. The CWT represents the convolution sum between a given signal $x(t)$ and the scaled mother wavelet $\psi(t)$.

Another formulation for the CWT of Eq. (1) can be represented as a product of the Fourier transform between $x(t)$ and $\psi^*_{u,s}(t)$:

$$W_\psi x(u,s) = \frac{\sqrt{s}}{2\pi}\int_{-\infty}^{\infty} X(\omega)\Psi^*(s\omega)\mathrm{e}^{\mathrm{i}\omega u}\,\mathrm{d}\omega, \tag{3}$$

where $X(\omega)$ and $\sqrt{s}\Psi^*(s\omega)\mathrm{e}^{\mathrm{i}\omega u}$ are the Fourier transform of $x(t)$ and the Fourier transform of $\psi^*_{u,s}(t)$, respectively.

The analytic wavelet function is used to separate the phase and amplitude information in the given signals. The mother wavelet $\psi(t)$ should satisfy the admissibility condition as follows:

$$C_\psi = \int_{-\infty}^{\infty} \frac{|\Psi(\omega)|^2}{|\omega|}\,\mathrm{d}\omega < \infty, \tag{4}$$

where $\Psi(\omega)$ is the Fourier transform of the mother wavelet $\psi(t)$.

The existence of the integral in Eq. (4) requires that

$$\int_{-\infty}^{\infty} \psi(t)\,\mathrm{d}t = 0, \quad \text{i.e. } \Psi(0) = 0. \tag{5}$$

Eqs. (4) and (5) mean that $\Psi(\omega)$ is the transfer function of a dilated band-pass filter in a frequency domain because $\Psi(\omega)$ converges to zero as an angular frequency increases to infinity.

Many mother wavelets have been employed in taking the CWT of a given signal. In analyzing the frequency evolution of a given signal, the CWT should use analytic wavelets such as the Gabor wavelet which has the smallest Heigenberg box [19]. In other words, the Gabor wavelet has the best time-frequency localization in analyzing the given signal using the CWT. The Gabor wavelet $\psi(t)$ can be constructed with a frequency modulation of a real and symmetric Gaussian window $g(t)$:

$$\psi(t) = g(t)\mathrm{e}^{\mathrm{i}\eta t} \tag{6}$$

with

$$g(t) = \frac{1}{(\sigma^2\pi)^{1/4}}\,\mathrm{e}^{(-t^2/2\sigma^2)} \tag{7}$$

where η is the center frequency of $\Psi(\omega)$ and σ is the measure of time spread of $\psi(t)$. The shape of the Gabor wavelet is controlled by the combination between η and σ. The Fourier transform of the Gaussian window is $G(\omega) = (4\pi\sigma^2)^{1/4}\mathrm{e}^{(-\sigma^2\omega^2/2)}$. If $\sigma^2\eta^2$ is much larger than one, then $G(\omega)$ is approximately zero for $|\omega| > \eta$. Such Gabor wavelets are then considered to be approximately analytic. The product of η and σ is called as the Gabor shaping factor $G_s = \sigma\eta$ [20].

In Eq. (3), the dilated version of the Fourier transform for the Gabor wavelet is defined as

$$\Psi(s\omega) = (4\pi\sigma^2)^{1/4}\mathrm{e}^{-\sigma^2(s\omega-\eta)^2/2}. \tag{8}$$

$\Psi(s\omega)$ of Eq. (8) has a maximum value at the center frequency of the mother wavelet, i.e., $s\omega = \eta$. This implies that the Gabor wavelet can be considered as a band-pass filter, because it has a fast decay at the frequency ranges outside of the center frequency.

3. Optimal shape determination of the mother wavelet

Before the calculation of the CWT of a given signal, the optimal Gabor shaping factor $G_{\mathrm{sopt}} = \sigma\eta$ should be chosen to ensure optimal resolution in both time and frequency. It is very important to choose the optimal Gabor shaping factor because it affects the time-frequency localization of the CWT based on the Gabor wavelet. The Shannon entropy theorem can be employed in order to determine the optimal Gabor shaping factor that gives the best time-frequency resolution of the CWT. The Shannon entropy can measure the uncertainty or the energy concentration quantity as the outcome of a random variable.

The one-dimensional Shannon entropy cost function $H_1(X_1)$ [19] of a random variable X_1 is given by

$$H_1(X_1) = -\sum_{k=1}^{K} p_k \log_2 p_k, \quad X_1 = \{x_k\}_{k=1,2,\ldots,K} \text{ and } p_k = \frac{|x_k|^2}{\|X_1\|^2}, \tag{9}$$

where p_k is the probability of the kth variable in the total energy and $H_1(X_1)$ is the uncertainty or the energy concentration level as the result of the random variable X_1. The range of $H_1(X_1)$ is

$$0 \le H_1(X_1) \le \log_2 K. \tag{10}$$

The maximum value of $\log_2 K$ implies that all variables have a uniform probability distribution, i.e., $p_k = 1/K$ for $1 \le k \le K$. Conversely, the minimum value, i.e., $H_1(X_1) = 0$, implies that the probability of a certain variable is one and the probability of the others is zero. In other words, the entropy is large if the energy is uniformly distributed on whole variables. On the other hand, the entropy is small if the energy is concentrated on certain variables.

If we apply the Shannon entropy theorem to the normalized scalogram $N_W x(u,s)$, which is defined as $|Wx(u,s)|^2/s$, we can obtain the two-dimensional normalized wavelet entropy:

$$H_2(X_2) = -\sum_{j=1}^{J} p_j \log_2 p_j, \tag{11}$$

where

$$X_2 = \{N_W x(u_k, s_j)\}_{\substack{k=1,2,\ldots,K \\ j=1,2,\ldots,J}} \quad \text{and} \quad p_j = \frac{\sum_{k=1}^{K} N_W x(u_k, s_j)}{\sum_{j=1}^{J}\sum_{k=1}^{K} N_W x(u_k, s_j)}. \tag{12}$$

Eventually, the optimal Gabor shaping factor G_{sopt} that minimizes the Shannon entropy cost function $H_2(X_2)$ of the normalized scalogram can be obtained by

$$G_{\text{sopt}} = \arg\left\{ \min_{G_s} H_2(X_2) \right\}. \tag{13}$$

The optimal Gabor shaping factor concentrates the energy of a given signal near the wavelet ridges.

4. Estimation of the beat characteristics and damping ratios using the CWT

4.1. The CWT of mono- and multi-spectral signals

Consider the wavelet transform for $x(t) = A(t)\cos(\varphi(t))$ of the single degree of freedom (SDOF) system where $A(t)$ and $\varphi(t)$ are an amplitude and a time-varying phase, respectively. If $x(t)$ is assumed to be an asymptotic signal, an analytic function of $x(t)$ is

$$x_a(t) = A(t)\mathrm{e}^{\mathrm{i}\varphi(t)}. \tag{14}$$

The wavelet transform based on the Gabor wavelet can be obtained as

$$W_\psi x(u,s) = \frac{1}{2}\langle x_a(t), \psi_{u,s}(t)\rangle = \frac{\sqrt{s}}{2} A(u)\mathrm{e}^{\mathrm{i}\varphi(u)} \left\{ G(\eta - s\varphi'(u)) + \varepsilon\left(u, \frac{\eta}{s}\right) \right\}, \tag{15}$$

where $G(\omega)$ is the Fourier transform of the Gaussian window function $g(t)$. Using $\Psi(\omega) = G(\omega - \eta)$, $G(\eta - s\varphi'(u))$ in Eq. (15) becomes $\Psi^*(s\varphi'(u))$. If $A(t)$ and $\varphi'(t)$ have small variation over the support of $\psi_{u,s}(t)$ and if $\varphi'(u)$ is larger than $\Delta\omega_\psi/s$ where $\Delta\omega_\psi$ is frequency bandwidth of the mother wavelet, the corrective term $\varepsilon(u, \eta/s)$ can be neglected. Therefore, Eq. (15) can be finally approximated as

$$W_\psi x(u,s) \cong \frac{\sqrt{s}}{2} A(u)\mathrm{e}^{\mathrm{i}\varphi(u)} \Psi^*(s\varphi'(u)). \tag{16}$$

Since $\Psi(s\omega)$ has a maximum value at $s\omega = \eta$, the absolute wavelet transform $|W_\psi x(u,s)|$ is maximum at $s(u)\varphi'(u) = \eta$, which are the wavelet ridge points. The wavelet ridges are a collection of corresponding points $(u,\varphi'(u))$, at which the normalized energy density called the wavelet scalogram becomes a local maximum at each time.

Consider that $x(t)$ is the response of the multi-degree of freedom (MDOF) system. The response of the N-DOF system can be expressed as a summation of the response of the SDOF system as follows:

$$x(t) = \sum_{k=1}^{N} x_k(t) = \sum_{k=1}^{N} A_k(t)\mathrm{e}^{\mathrm{i}\varphi_k(t)}, \quad k = 1, 2, \ldots i-1, i, i+1, \ldots, N, \tag{17}$$

where $A_k(t)$ and $\varphi_k(t)$ are an amplitude and a time-varying phase of $x_k(t)$, respectively.

Since the CWT is a linear transformation of a given signal, the CWT of the signal with the multi-spectral components is given by the summation of that of SDOF signal:

$$W_\psi x(u,s) = W_\psi \left\{ \sum_{k=1}^{N} x_k(u,s) \right\} \cong \sum_{k=1}^{N} \frac{\sqrt{s}}{2} A_k(u)\,\mathrm{e}^{\mathrm{i}\varphi_k(u)} \Psi^*(s_k\varphi_k'(u)), \tag{18}$$

where if the dilated window has an enough frequency resolution at the wavelet ridge scales, which are $s_i = \eta/\varphi_i'(u)$ and $s_{i+1} = \eta/\varphi_{i+1}'(u)$, the instantaneous frequencies $\varphi_i'(t)$ and $\varphi_{i+1}'(t)$ do not interfere with the wavelet ridges of $\varphi_i'(t)$ and $\varphi_{i+1}'(t)$ each other:

$$\frac{|\varphi_i'(u) - \varphi_{i+1}'(u)|}{\varphi_i'(u)} \geq \frac{\Delta\omega_\psi}{\eta} \tag{19a}$$

and

$$\frac{|\varphi_i'(u) - \varphi_{i+1}'(u)|}{\varphi_{i+1}'(u)} \geq \frac{\Delta\omega_\psi}{\eta}. \tag{19b}$$

The two spectral components of a signal $x(t)$, which are very close, can effectively be separated by selecting a very small value for an octave bandwidth $(\Delta\omega_\psi/\eta)$. In other words, either a very big center frequency η should be selected when calculating the CWT of a signal $x(t)$ or a very small bandwidth $\Delta\omega_\psi$ should be chosen. However, an adequate center frequency η for the Gabor wavelet should be selected. Although the selection of a big center frequency gives a very narrow

frequency resolution, the time resolution is not very good in the CWT when using the Gabor wavelet. For this reason, when applying the Gabor wavelet for the CWT analysis, the optimal center frequency η and optimal time spread σ, which can be obtained by the Shannon wavelet entropy theorem, should be selected to well decouple the given signal into each mode because the size of the Heigenberg box for the Gabor wavelet is fixed by $\frac{1}{2}$ [19].

In Eq. (18), if we choose the optimal Gabor shaping factor in order to have sufficient frequency resolution, we can decouple the close natural modes. In other words, because the mother wavelet function has compact support in the frequency and time domains, the wavelet transform at the scale parameter s_i associated with the ith dynamic mode can only provide a relevant contribution. On the other hand, at a scale parameter not associated with the ith dynamic mode, the wavelet transform cannot provide any contribution:

$$\Psi^*(s_k\varphi_k'(u)) = 0 \quad \text{for } k = 1,2,\ldots,i-1,\ i+1,\ldots,N. \tag{20}$$

Thus, the wavelet transform of the MDOF system can be decoupled into each mode of the SDOF system:

$$W_\psi x_i(u,s_i) = \frac{\sqrt{s_i}}{2} A_i(u)\, e^{i\varphi_i(u)}\, \Psi^*(s_i\varphi_i'(u)). \tag{21}$$

Finally, the mode decoupling procedure of the MDOF system is effectively accomplished by the CWT.

4.2. Extracting the beat characteristics and damping ratios of bell type structures

The most important characteristics of a Korean bell are its beat characteristics and a long duration in its sound. Such a Korean bell can be mathematically modeled as a slightly asymmetric cylindrical shell or circular ring. By the impulse response analysis, the beat response of each (m, n) mode in a slightly asymmetric cylindrical shell is given by [1]

$$\begin{aligned} u_{3mn}(x^*,\theta,t) = e^{-\zeta_{mna}\omega_{mna}t}\{&\cos n(\theta^* - \varphi_{mnL})\cos n(\theta - \varphi_{mnL})\sin(\omega_{mnL}t) \\ &+ \cos n(\theta^* - \varphi_{mnH})\cos n(\theta - \varphi_{mnH})\sin(\omega_{mnH}t)\}, \end{aligned} \tag{22}$$

where ω_{mnH} and ω_{mnL} are the natural frequency of the high mode and the natural frequency of the low mode, respectively. Subscripts m and n mean the mode sequence of the longitudinal direction and the mode sequence of the radial direction in the Korean bell, respectively. θ^* is the position of the striking point. φ_{mnH} and φ_{mnL} are the position of the anti-node for the high mode and the position of the anti-node for the low mode, respectively. The phase difference between the low and high mode in a certain mode pair is given by

$$\varphi_{mnH} = \varphi_{mnL} + \frac{\pi}{2n}, \quad n = 2,3,4,\ldots,\infty. \tag{23}$$

The average values of frequency and damping are used as follows, since these values for each mode pair are almost the same:

$$\omega_{mna} = (\omega_{mnL} + \omega_{mnH})/2 \quad \text{and} \quad \zeta_{mna} = (\zeta_{mnL} + \zeta_{mnH})/2. \tag{24}$$

By using Eq. (21), the CWT for a certain mode (m, n) of a slightly asymmetric cylindrical shell, as is shown in Eq. (22), is given by

$$W_\psi u_{3mn}(u,s) = W_\psi u_{3mnL}(u,s) + W_\psi u_{3mnH}(u,s), \tag{25}$$

where

$$W_\psi u_{3mnL}(u,s) = \frac{C_{mnL}}{2}\sqrt{s}\, e^{-\zeta_{mna}\omega_{mna}u}\, \Psi^*(s\omega_{mnL})\, e^{i\omega_{mnL}u}, \tag{26}$$

$$W_\psi u_{3mnH}(u,s) = \frac{C_{mnH}}{2}\sqrt{s}\, e^{-\zeta_{mna}\omega_{mna}u}\, \Psi^*(s\omega_{mnH})\, e^{i\omega_{mnH}u}, \tag{27}$$

$$C_{mnL} = \cos n(\theta^* - \varphi_{mnL})\cos n(\theta - \varphi_{mnL}), \tag{28a}$$

$$C_{mnH} = \cos n(\theta^* - \varphi_{mnH})\cos n(\theta - \varphi_{mnH}). \tag{28b}$$

Here, C_{mnL} and C_{mnH} are the contribution factor of the low mode $(m, n)_L$ and the contribution factor of the high mode $(m, n)_H$ contributing to the beat response, respectively.

Since the dilated mother wavelet function $\Psi(s_{\omega_{mna}}\omega)$ is a symmetric function at the center frequency η on the x-axis, $\Psi^*(s_{\omega_{mna}}\omega_{mnL})$ is equal to $\Psi^*(s_{\omega_{mna}}\omega_{mnH})$ where $s_{\omega_{mna}}$ is the scale parameter corresponding to the average frequency ω_{mna} of the low and high mode. Thus, at the average frequency ω_{mna}, Eq. (25) becomes

$$\begin{aligned} W_\psi u_{3mn}(u,s_{\omega_{mna}}) &= \frac{\sqrt{s_{\omega_{mna}}}}{2}\, e^{-\zeta_{mna}\omega_{mna}u}\, \Psi^*(s_{\omega_{mna}}\omega_{mnL})\{C_{mnL}\, e^{i\omega_{mnL}u} + C_{mnH}\, e^{i\omega_{mnH}u}\} \\ &= \frac{\sqrt{s_{\omega_{mna}}}}{2}\, e^{-\zeta_{mna}\omega_{mna}u}\, \Psi^*(s_{\omega_{mna}}\omega_{mnL}) R_{mn}\, e^{i\Theta_{mn}}, \end{aligned} \tag{29}$$

where

$$R_{mn} = \sqrt{C_{mnL}^2 + C_{mnH}^2 + 2C_{mnL}C_{mnH}\cos\{(\omega_{mnH} - \omega_{mnL})u\}}, \tag{30}$$

$$\Theta_{mn} = \tan^{-1}\left(\frac{C_{mnL}\sin\omega_{mnL}u + C_{mnH}\sin\omega_{mnH}u}{C_{mnL}\cos\omega_{mnL}u + C_{mnH}\cos\omega_{mnH}u}\right). \tag{31}$$

In order to obtain the modulus of the wavelet transform, we must take the absolute value for $W_\psi u_{3mn}(u, s_{\omega_{mna}})$:

$$|W_\psi u_{3mn}(u, s_{\omega_{mna}})| = \frac{\sqrt{s_{\omega_{mna}}}}{2}\, e^{-\zeta_{mna}\omega_{mna}u}\,|\Psi^*(s_{\omega_{mna}}\omega_{mnL})R_{mn}|, \tag{32}$$

In Eq. (32), the envelope of the wavelet modulus $|W_\psi u_{3mnL}(u, s_{\omega_{mna}})|$ at ω_{mna} is the function of $\cos\{(\omega_{mnH}-\omega_{mnL})u\}$. The period of the amplitude-modulated envelope in the wavelet modulus indicates the beat period of the (m, n) beating mode:

$$T_{mn} = \frac{4\pi}{\omega_{mnH} - \omega_{mnL}}. \tag{33}$$

In order to extract the damping ratio of the (m, n) mode associated with the beat response, we take a semi-logarithm of the wavelet modulus $|W_\psi u_{3mn}(u, s_{\omega_{mna}})|$ to obtain the following:

$$\ln|W_\psi u_{3mn}(u, s_{\omega_{mna}})| = -\zeta_{mna}\omega_{mna}u + \ln\left\{\frac{\sqrt{s_{\omega_{mna}}}}{2}\,|\Psi^*(s_{\omega_{mna}}\omega_{mnL})R_{mn}|\right\}, \tag{34}$$

The damping ratios of a given signal $u_{3mn}(t)$ can be identified by calculating the slope of the straight line having a translation parameter u as an independent variable on the semi-logarithm of the wavelet modulus.

If C_{mnL} is equal to C_{mnH}, i.e., an in-phase contribution of a low $(m, n)_L$ and high mode $(m, n)_H$ to a beat response of the (m, n) mode, Eq. (29) can be rewritten as

$$W_\psi u_{3mn}(u, s_{\omega_{mna}}) = C_{mnL}\sqrt{s_{\omega_{mna}}}\, e^{-\zeta_{mna}\omega_{mna}u}\,\Psi^*(s_{\omega_{mna}}\omega_{mnL})\cos\alpha_{mn}\, e^{i\beta_{mn}}, \tag{35}$$

where

$$\alpha_{mn} = (\omega_{mnH} - \omega_{mnL})u/2 \tag{36a}$$

and

$$\beta_{mn} = (\omega_{mnH} + \omega_{mnL})u/2. \tag{36b}$$

If C_{mnL} is equal to $-C_{mnH}$, i.e., an out-of-phase contribution of a low $(m, n)_L$ and high mode $(m, n)_H$ to beat response of the (m, n) mode, Eq. (29) can be rewritten as

$$W_\psi u_{3mn}(u, s_{\omega_{mna}}) = -iC_{mnL}\sqrt{s_{\omega_{mna}}}\, e^{-\zeta_{mna}\omega_{mna}u}\,\Psi^*(s_{\omega_{mna}}\omega_{mnL})\sin\alpha_{mn}\, e^{i\beta_{mn}}. \tag{37}$$

As can be seen in Eq. (35), when the contribution of the low and high mode contributing to the beat response is the same, the wavelet modulus shows the function of $\cos\alpha_{mn}$ at the average frequency between the low and high mode. On the other hand, as can be seen in Eq. (37), if the contribution of the low and high mode contributing to the beat response is out-of-phase, the wavelet modulus is the function of $\sin\alpha_{mn}$. In the same manner, the period of the envelope in the wavelet modulus is $T_{mn} = 4\pi/(\omega_{mnH} - \omega_{mnL})$.

In Eqs. (35) and (37), the argument of $W_\psi u_{3mn}(u, s_{\omega_{mna}})$ is given by

$$\arg\{W_\psi u_{3mn}(u, s_{\omega_{mna}})\} = (\omega_{mnH} + \omega_{mnL})u/2. \tag{38}$$

If we take a derivative with respect to the translation parameter for Eq. (38), the average value of the low and high frequency for the (m, n) mode can be obtained as

$$\omega_{mna} = \frac{d}{du}\arg\{W_\psi u_{3mn}(u, s_{\omega_{mna}})\} = (\omega_{mnH} + \omega_{mnL})/2. \tag{39}$$

Finally, the natural frequencies of the low mode ω_{mnL} and high mode ω_{mnH} for the (m, n) mode can be obtained from Eqs. (33) and (39), respectively.

$$\omega_{mnL} = \omega_{mna} - \frac{2\pi}{T_{mn}} \tag{40a}$$

and

$$\omega_{mnH} = \omega_{mna} + \frac{2\pi}{T_{mn}}. \tag{40b}$$

If either C_{mnL} or C_{mnH} is zero, i.e., the response or excitation point is located on the nodal line of the low or high mode of the (m, n) mode, then the wavelet transform of each mode can be simply obtained as follows:

$$W_\psi u_{3mn}(u,s) = \begin{cases} \frac{C_{mnL}}{2}\sqrt{s}\, e^{-\zeta_{mnL}\omega_{mnL}u}\, \Psi^*(s\omega_{mnL})\, e^{i\omega_{mnL}u} & \text{for low mode,} \\ \frac{C_{mnH}}{2}\sqrt{s}\, e^{-\zeta_{mnH}\omega_{mnH}u}\, \Psi^*(s\omega_{mnH})\, e^{i\omega_{mnH}u} & \text{for high mode.} \end{cases} \tag{41a,b}$$

At the nodal line of the high mode of each (m, n) mode, the modal damping ratio for the low mode can be obtained by calculating the slope of the straight line of the wavelet modulus:

$$\ln|W_\psi u_{3mn}(u, s_{\omega_{mnL}})| = -\zeta_{mnL}\omega_{mnL}u + \ln\left\{\frac{C_{mnL}}{2}\sqrt{s_{\omega_{mnL}}}|\Psi^*(s_{\omega_{mnL}}\omega_{mnL})|\right\}. \tag{42}$$

Similarly, at the nodal line of the low mode of each (m, n) mode, the modal damping ratio for the high mode can be obtained by calculating the slope of the straight line of the wavelet modulus:

$$\ln|W_\psi u_{3mn}(u, s_{\omega_{mnH}})| = -\zeta_{mnH}\omega_{mnH}u + \ln\left\{\frac{C_{mnH}}{2}\sqrt{s_{\omega_{mnH}}}|\Psi^*(s_{\omega_{mnH}}\omega_{\omega_{mnH}})|\right\}. \tag{43}$$

As can be seen in Eqs. (42) and (43), we cannot observe any period of the wavelet modulus because the response or excitation point is placed on the nodal line of each mode.

Similarly, the low or high frequency of the (m, n) mode can be obtained by computing the derivative of the argument of the wavelet transform in Eq. (41a,b):

$$\omega_{mnL} = \frac{d}{du}\arg\{W_\psi u_{3mn}(u, s_{\omega_{mnL}})\} \tag{44a}$$

and

$$\omega_{mnH} = \frac{d}{du}\arg\{W_\psi u_{3mn}(u, s_{\omega_{mnH}})\}. \tag{44b}$$

5. Simulation results and discussion

In this section, we examine the effectiveness of the proposed method with a simulated model in identifying the beat characteristics and modal damping ratios of the bell type structures using the CWT. As previously stated, the most remarkable characteristics of a Korean bell are the beat phenomenon and long time duration for its vibration and sound. In order to identify the beat and damping ratio associated with the time duration, we simulated the dynamic system with the beat phenomenon and the modal damping using Eq. (22). In this paper, the MATLAB program was used for the calculation of the CWT. For the simulation, the contribution factors of the low and high mode contributing to the beating response of the (m, n) mode, the modal damping ratios and the natural frequencies of the low and high mode are given in Table 1. As is listed in Table 1, because the contribution of the $(1,2)_H$ mode and the contribution of the $(0,4)_L$ mode are zero, the mode pairs contributing to the beating response are the only three modes, which are the $(0,2)$, $(0,3)$ and $(1,3)$ mode. Each modal response of the simulated model is expressed in time domain, as is shown in Fig. 1. The total sum of the modal response is shown in Fig. 2. In this section, the simulation using the wavelet transform was carried out in two cases, which are the pure signal and the signal to noise ratio (SNR) 5 dB noisy signal. In Fig. 2, the black line and gray line indicate the pure signal without any noise and SNR 5 dB noisy signal, respectively.

Table 1
Description of the simulated signal.

Mode sequence	Contribution factor of each mode (C_{mnL}, C_{mnH})	Damping ratio (ζ_{mn})	Natural frequency (Hz)
$(0,2)_L$	1.5	0.00009	90.69
$(0,2)_H$	1.5	0.00011	91.62
$(0,3)_L$	0.4	0.00029	170.71
$(0,3)_H$	−0.4	0.00031	171.22
$(1,2)_L$	0.35	0.00032	309.57
$(1,2)_H$	0	–	–
$(1,3)_L$	−0.3	0.00035	358.62
$(1,3)_H$	0.3	0.00037	359.91
$(0,4)_L$	0	–	–
$(0,4)_H$	0.25	0.00038	403.23

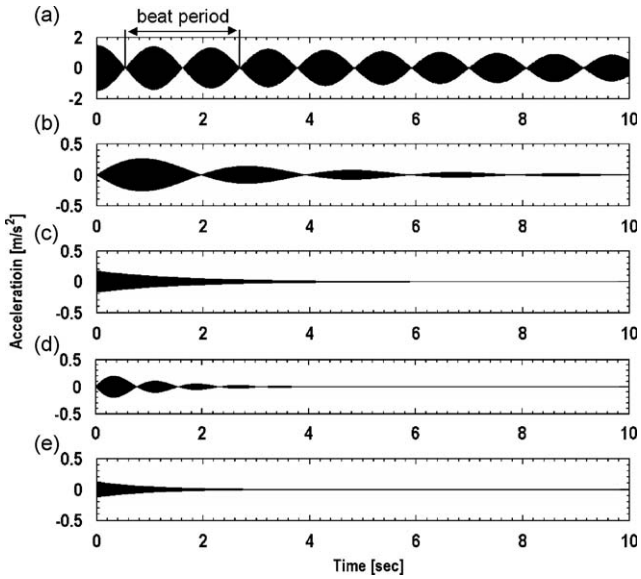

Fig. 1. Each modal response contributing to the beat phenomenon: (a) $(0,2)$ mode; (b) $(0,3)$ mode; (c) $(1,2)$ mode; (d) $(1,3)$ mode; (e) $(0,4)$ mode.

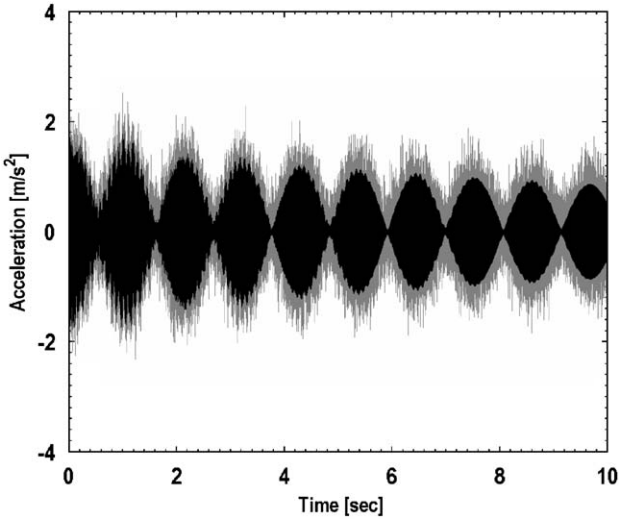

Fig. 2. The summation of each modal response. (—) pure signal and (——) SNR 5 dB noisy signal.

First of all, the optimal Gabor shaping factor which gives the best time frequency localization in taking the CWT of the simulated signal was obtained using the Shannon entropy cost function as previously stated. Under the constant center frequency η for the Gabor wavelet, the time spread σ of the Gaussian window was set as an independent variable. In this simulation, the center frequency η satisfying the admissibility condition of Eq. (4) was selected to be 4π. In the case of the pure signal, the optimal time spread σ of Gaussian window obtained from the Shannon entropy was determined to be $\sqrt{13/2}$, as is shown in Fig. 3. The obtained optimal time spread σ_{opt} gives the Shannon wavelet entropy its lowest value. Using the optimal Gabor shaping factor G_{sopt}, we carried out the CWT on the pure signal, as is shown in Fig. 4. The two-dimensional wavelet modulus contour shown in Fig. 4 has three beating modes and two exponential decay modes at each natural frequency. The ridge lines, which correspond to the local maximum of wavelet modulus, indicate the average frequency of the low and high mode for the (m, n) mode. The wavelet modulus plots are shown in Figs. 5(a) and (c) in time domain at each average frequency of the (m, n) beating mode. Because the first beating mode $(0,2)$ is in-phase contribution from the low and high mode, Fig. 5(a) indicates a cosine wave for the wavelet magnitude, as is described in Eq. (35). On the other hand, because the second beating mode $(0,3)$ consists of an out-of-phase contribution between the low and high mode, Fig. 5(c) shows a sine wave as the magnitude of the wavelet modulus, as is shown in Eq. (37). Using Eq. (33), we

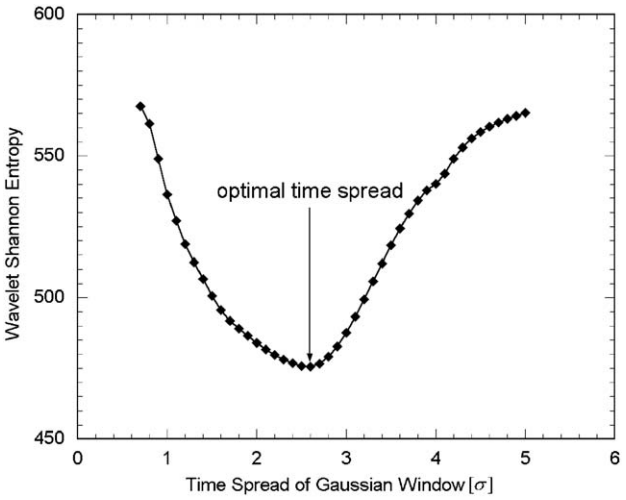

Fig. 3. The Shannon wavelet entropy of the simulated signal.

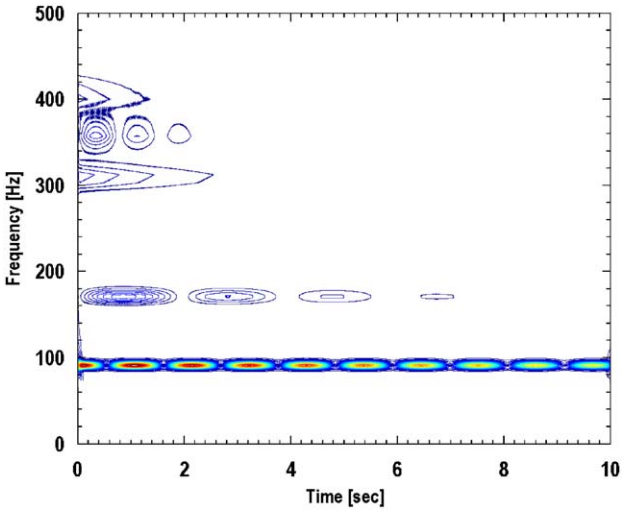

Fig. 4. The two-dimensional wavelet modulus of the simulated signal.

extracted the beat periods from these wavelet modulus graphs, as are listed in Table 2. Similarly, we extracted the beat periods of each mode in case of SNR 5 dB noisy signal. The extracted beat periods of the two cases, which are the pure and noisy signal, are in close agreement with the given values. As is listed in Table 3, the low and high natural frequency related to the (m, n) beating mode were obtained from Eqs. (39) and (40), and the low or high natural frequency of the (m, n) mode not related to the beating response was obtained by Eq. (44). In the two cases which are the pure signal and the SNR 5 dB noisy signal, the acquired natural frequencies are in close agreement with the given values.

Next, we can use Eqs. (34), (42) and (43) in order to obtain the modal damping ratios of the simulated signals. Eq. (34) is suitable in extracting the modal damping ratios of the beating mode, and Eqs. (42) and (43) are effective for extracting those ratios when either the contribution of the low mode or the contribution of the high mode is zero. Figs. 5(b) and (d) are the semi-logarithms of the wavelet modulus at each average frequency between the high and low mode. Finally, we identified the modal damping ratio using the slope of the semi-logarithm of the wavelet modulus, as is listed in Table 4. Regarding the case of the pure and noisy signal, the results obtained in Table 4 are in very good agreement with the given values.

So far, we have verified the validity of the proposed method in identifying the beat period, the modal damping ratio and the natural frequency of the simulated signal with the mode pairs. Even if the simulated signal was seriously contaminated by noise, the proposed method gave us very reliable results. We especially confirmed that the CWT is very convenient and reliable tool in performing the mode decoupling procedure when we identify the modal parameters of the bell type structures.

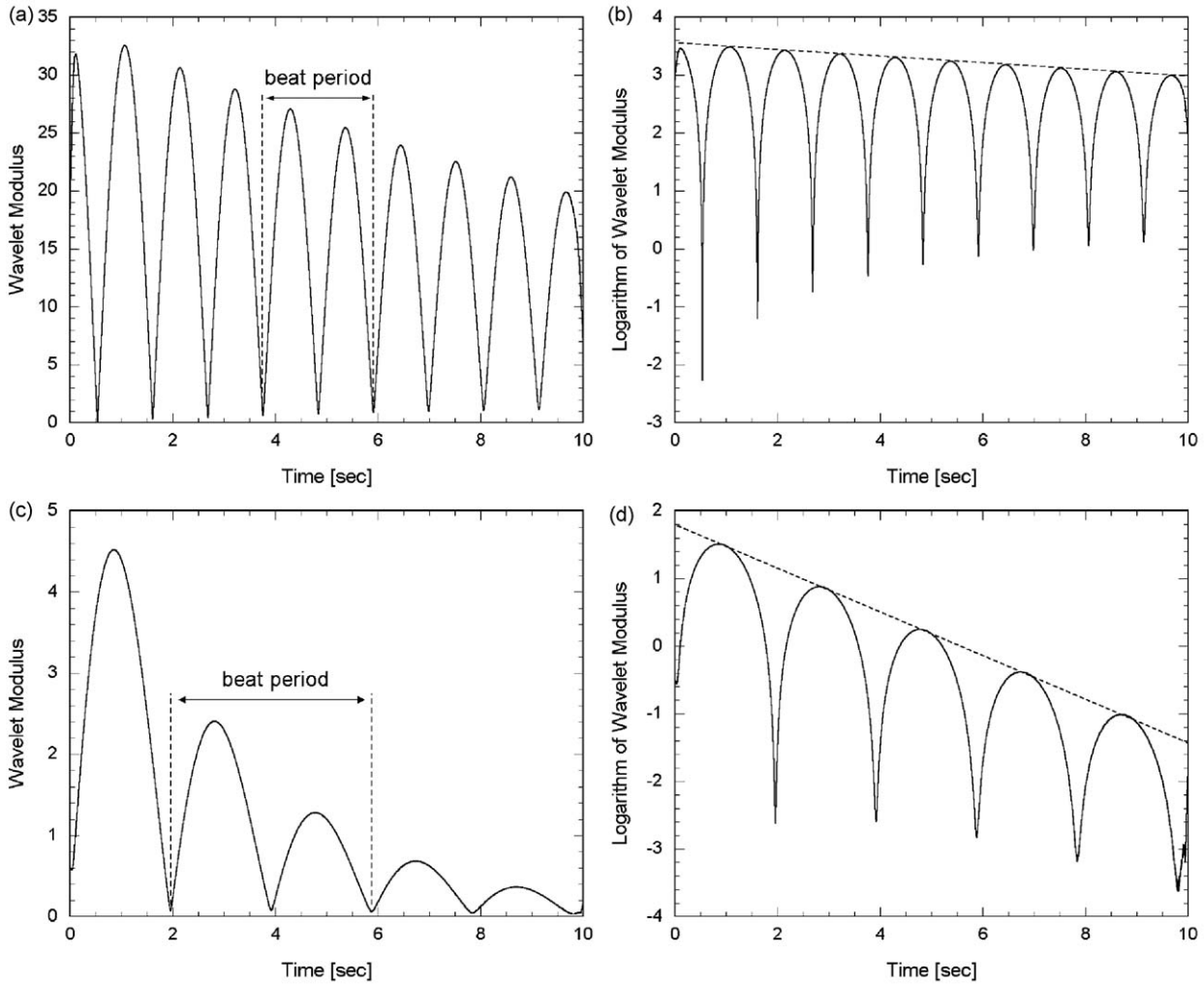

Fig. 5. The wavelet modulus and its semi-logarithm of the simulated signal: (a) wavelet modulus of (0, 2) mode; (b) semi-logarithm of (0, 2) mode; (c) wavelet modulus of (0, 3) mode; (d) semi-logarithm of (0, 3) mode.

Table 2
Estimated beat period of the pure and SNR 5 dB signal.

Mode sequence	Given beat period (s)	Beat period obtained by the CWT (s)	
		Pure signal	SNR 5 dB noisy signal
(0, 2)	2.151	2.151	2.150
(0, 3)	3.922	3.922	3.922
(1, 2)	0	0	0
(1, 3)	1.550	1.551	1.551
(0, 4)	0	0	0

6. Experimental results and discussion

In previous section, we investigated the validity of the proposed method in identifying the beat characteristics and damping ratios of the bell type structure. In this section, we applied the proposed method to a small-sized Korean bell (small-scale Bosingak bell) to verify its applicability in the field. The dimensions of the bell used for an experiment and experimental setup for impact testing are described in Fig. 6. The external force of the bell was excited by an ENDEVCO 2302-10 impact hammer with a rubber tip, and acceleration signals from the bell were measured using a PCB

Table 3
Estimated natural frequency of the pure and SNR 5 dB signal.

Mode sequence	Given values (Hz)	Pure signal (Hz)	SNR 5 dB noisy signal (Hz)
$(0,2)_L$	90.69	90.69	90.69
$(0,2)_H$	91.62	91.62	91.62
$(0,3)_L$	170.71	170.69	170.69
$(0,3)_H$	171.22	171.20	171.20
$(1,2)_L$	309.57	309.64	309.64
$(1,2)_H$	–	–	–
$(1,3)_L$	358.62	358.42	358.42
$(1,3)_H$	359.91	359.71	359.71
$(0,4)_L$	–	–	–
$(0,4)_H$	403.23	403.18	403.18

Table 4
Estimated modal damping ratio of the pure and SNR 5 dB signal.

Mode sequence	Averaged modal damping ratio (ζ_{mna})		
	Given values	Pure signal	SNR 5 dB noisy signal
(0, 2)	0.00010	0.0000999	0.0000998
(0, 3)	0.00030	0.000301	0.000299
(1, 2)	0.00032	0.000320	0.000320
(1, 3)	0.00036	0.000359	0.000359
(0, 4)	0.00038	0.000381	0.000381

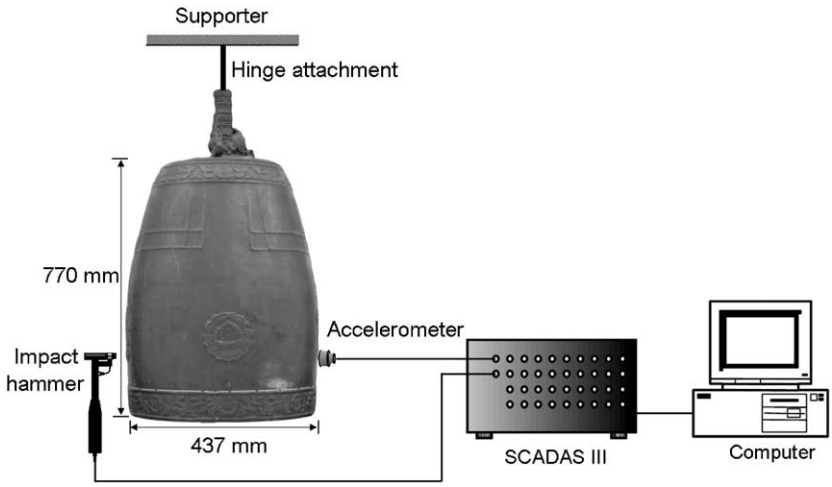

Fig. 6. The geometry dimensions of a Korean bell and experimental setup for an impact testing.

352C22 uni-axial accelerometer. Impact signals of the bell were gathered by LMS analyzer system (Test.Lab and SCADAS III). Because the amplitude and the phase of the low and high mode contributing to beating response of (m, n) mode in a bell are different from one position to another position, the determination of measurement point and striking position is very important in accurately measuring the beat response of each mode [1]. In this paper, the striking position of the impact hammer and the measurement position by the accelerometer are illustrated in Fig. 7.

First, we chose Impact 1 as the first striking position and Measurement 1 as the first measurement position. The temporal response under the impact testing is shown in Fig. 8. Before performing the CWT of the measured signal, the optimal Gabor shaping factor was obtained using the Shannon wavelet entropy. In this simulation, we selected the center frequency to be 12π, and then the optimal time spread σ of the Gaussian window was determined to be three, as is shown in Fig. 9.

Using the optimal Gabor shaping factor G_{sopt} obtained from Eq. (13), we carried out the CWT on the measured signal, as is shown in Fig. 10. The wavelet modulus contour shown in Fig. 10 has two beating modes, which are the (0, 2) mode and

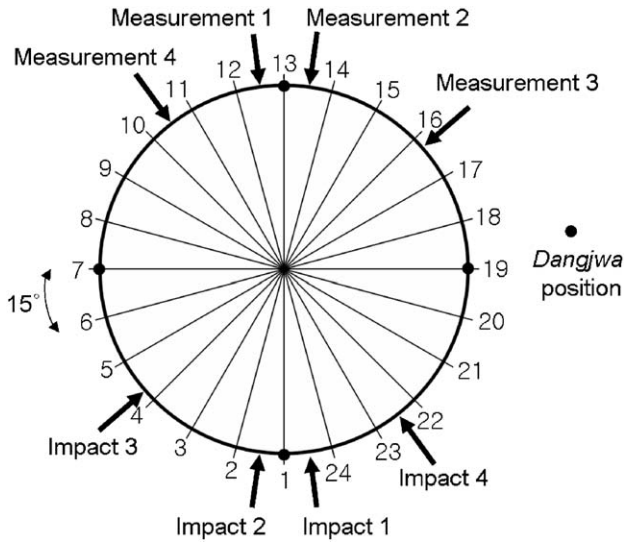

Fig. 7. The positions of impact and measurement (top view).

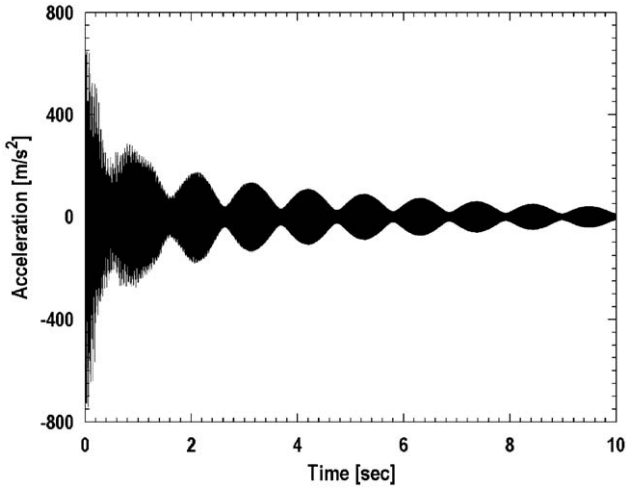

Fig. 8. The temporal response under the impact testing.

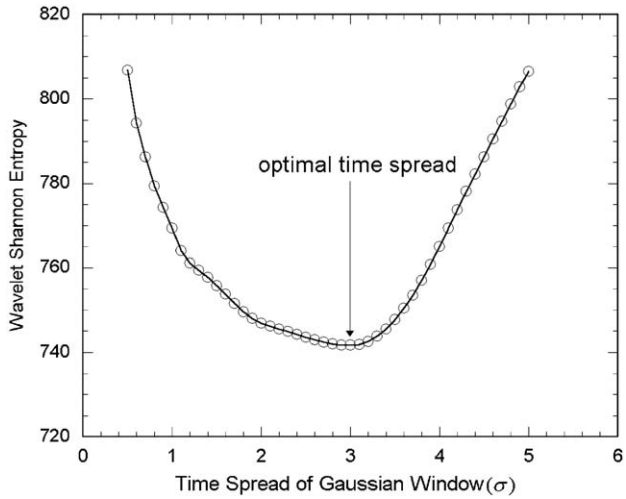

Fig. 9. The wavelet Shannon entropy of the measured signal.

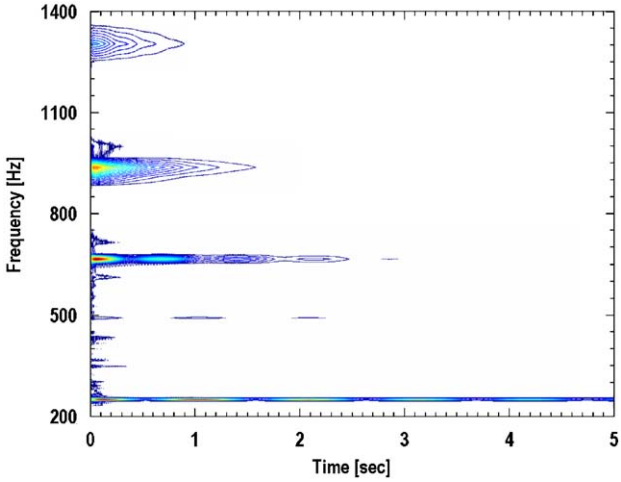

Fig. 10. The two-dimensional wavelet modulus of the measured signal.

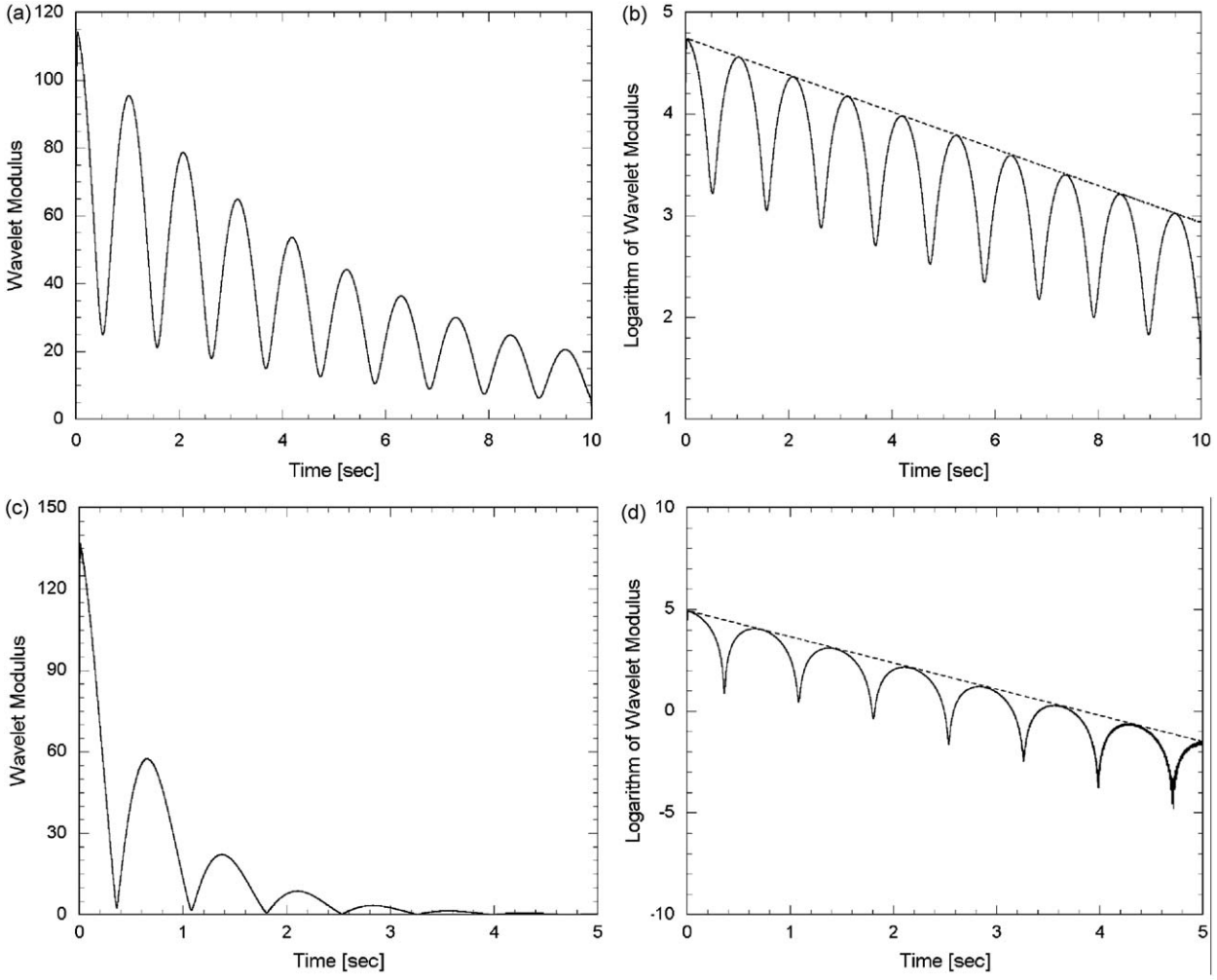

Fig. 11. The wavelet modulus and its semi-logarithm of the measured signal: (a) wavelet modulus of $(0,2)$ mode; (b) semi-logarithm of $(0,2)$ mode; (c) wavelet modulus of $(0,3)$ mode; (d) semi-logarithm of $(0,3)$ mode.

(0, 3) mode, and four exponential decay modes, which are the (1, 2) mode, (1, 3) mode, (0, 4) mode and (1, 4) mode. We extracted the wavelet modulus at the first and second average frequency, and then we took the semi-logarithm for estimating the beat periods, natural frequencies and modal damping ratios of the low and high mode shown in Fig. 11. As shown in Fig. 11(a), because the wavelet modulus for the (0, 2) beating mode shows a cosine wave, the contribution of the low and high mode contributing to the (0, 2) beating response is in-phase at the position of Measurement 1. However, the contribution of the low and high mode contributing to the (0, 3) beating response is out-of-phase at the position of Measurement 1 because the wavelet modulus for the (0, 3) beating mode is a sine wave, as is shown in Fig. 11(c). As shown in Fig. 10, the wavelet modulus diagram of the response measured at Measurement 1 has only the exponential decay response characteristics in the frequency range of the third and fourth beating mode. For this reason, we cannot obtain the beat characteristics such as beat period and modal damping ratio at the third and fourth beating mode. In order to obtain the beat characteristics and modal damping ratio of the third and fourth beating mode, we chose Impact 2 for the excitation of the bell and Measurement 2 for measuring the beating response. Similarly, we estimated the damping ratios, natural frequencies and beat periods at the third and fourth average frequency on the wavelet modulus contour and its

Table 5
Estimated beat period of the measured signal.

Mode sequence	Estimated beat period (s)	Estimated averaged frequency (Hz)
(0, 2)	2.110	250.00
(0, 3)	1.448	666.67
(1, 2)	0.809	911.85
(1, 3)	0.770	940.44
(0, 4)	0.943	1003.30
(1, 4)	0.497	1295.90

Table 6
Estimated natural frequency of the measured signal.

Mode sequence	Natural frequency using Eq. (40) (Hz)	Natural frequency using Eq. (44) (Hz)	Difference (%)
$(0,2)_L$	249.53	249.69	−0.063
$(0,2)_H$	250.47	250.63	−0.062
$(0,3)_L$	665.98	665.93	0.008
$(0,3)_H$	667.36	667.41	−0.007
$(1,2)_L$	910.62	910.47	0.016
$(1,2)_H$	913.09	913.24	−0.017
$(1,3)_L$	939.14	938.97	0.018
$(1,3)_H$	941.74	941.92	−0.019
$(0,4)_L$	1002.24	1001.67	0.057
$(0,4)_H$	1004.36	1003.34	0.101
$(1,4)_L$	1293.89	1293.10	0.061
$(1,4)_H$	1297.91	1298.70	−0.061

Table 7
Estimated modal damping ratio of the measured signal.

Mode sequence	Modal damping ratio using Eq. (34)	Modal damping ratio using Eqs. (42) and (43)	
(0, 2)	0.00011	$(0,2)_L$	0.00013
		$(0,2)_H$	0.00011
(0, 3)	0.00030	$(0,3)_L$	0.00032
		$(0,3)_H$	0.00029
(1, 2)	0.00045	$(1,2)_L$	0.00043
		$(1,2)_H$	0.00047
(1, 3)	0.00036	$(1,3)_L$	0.00037
		$(1,3)_H$	0.00036
(0, 4)	0.00043	$(0,4)_L$	0.00044
		$(0,4)_H$	0.00043
(1, 4)	0.00032	$(1,4)_L$	0.00033
		$(1,4)_H$	0.00032

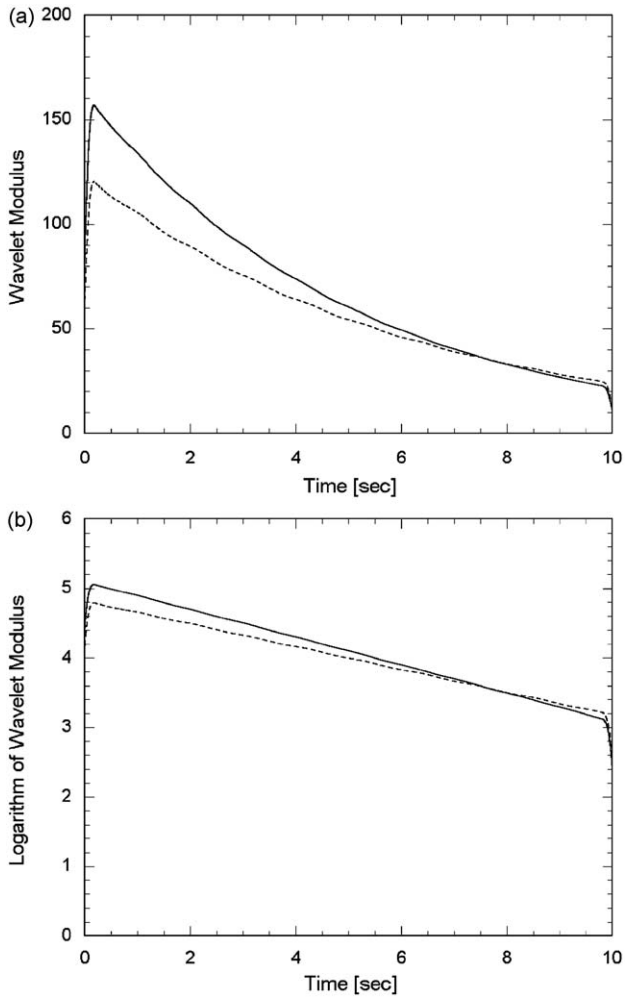

Fig. 12. The wavelet modulus (a) of the first low $(0,2)_L$ and high mode $(0,2)_H$ in the measured signal and its semi-logarithm (b). (—) the first low mode, (- - -) the first high mode.

semi-logarithm, as are listed in Tables 5 and 6. For the fifth and sixth beating mode, we chose Impact 3 as the impact location and Measurement 3 as the measurement position. Table 6 shows the low and high natural frequency of each beating mode calculated by Eqs. (40) and (44). The natural frequencies of the low and high mode obtained from Eq. (40) were well agreed with those obtained from Eqs. (44). Table 7 shows the modal damping ratios obtained by Eqs. (34), (42) and (43). Similarly, the modal damping ratios by Eq. (34) were in good agreement with those by Eqs. (42) and (43). Especially, the modal damping ratio and natural frequency of the first low mode were obtained at the position of Measurement 4 under the excitation of Impact 4, and those of the first high mode were obtained at the position of Measurement 2 under the excitation of Impact 2. Fig. 12 shows the wavelet modulus and its semi-logarithm of the signals measured from Measurements 4 and 2. Namely, Measurements 4 and 2 are located on the nodal line of the high mode $(0,2)_H$ and the nodal line of the low mode $(0,2)_L$, respectively. Finally, the modal damping ratios and natural frequencies calculated by Eqs. (34) and (40) are in good agreement with those results obtained from Eqs. (42)–(44).

7. Conclusions

In this paper, we proposed an effective method for estimating the beat characteristics and modal damping ratios of a Korean bell using the continuous wavelet transform. The modal decoupling procedure of a beating signal was effectively carried out using the CWT based on the Gabor wavelet. Before taking the CWT for a beating signal, the optimal shape of the Gabor wavelet was determined by employing the Shannon entropy cost function. The optimal Gabor shaping factor, which gives the best time frequency resolution in the CWT of a given signal, was applied to a pure and noisy signal. In an example simulation, the effectiveness of the CWT was verified in identifying the beat characteristics and damping characteristics of a simulated beating response. The beat characteristics, which are the beat period, the beating frequency and the phase of

the low and high mode contributing to the beating response, were estimated from the wavelet modulus of a given signal. The modal damping ratio of each mode was also extracted from the slope of the semi-logarithm of the wavelet modulus. Finally, we performed the experiment with a Korean bell. The results obtained from the CWT of the experimental signal confirmed the effectiveness of the proposed method.

Acknowledgements

This work was supported by Institute of Advanced Machinery and Design at Seoul National University and Brain Korea 21 Project of the Ministry of Education, Republic of Korea.

References

[1] S.H. Kim, C.W. Lee, J.M. Lee, Beat characteristics and beat maps of the King Seong-deok Divine Bell, *Journal of Sound and Vibration* 281 (2005) 21–44.
[2] J.M. Lee, S.H. Kim, S.J. Lee, J.D. Jeong, H.G. Choi, A study on the vibration characteristics of a large size Korean bell, *Journal of Sound and Vibration* 257 (4) (2002) 779–790.
[3] T. Charnley, R. Perrin, Studies with an eccentric bell, *Journal of Sound and Vibration* 58 (1978) 517–525.
[4] R. Perrin, T. Charnley, H. Bandu, Increasing the lifetime of warble-suppressed bells, *Journal of Sound and Vibration* 80 (1982) 298–303.
[5] S.H. Kim, W. Soedel, J.M. Lee, Analysis of the beating response of bell type structures, *Journal of Sound and Vibration* 173 (4) (1994) 517–536.
[6] T.D. Rossing, A. Perrier, Modal analysis of a Korean bell, *Journal of the Acoustical Society of America* 94 (4) (1993) 2431–2433.
[7] J.S. Hong, J.M. Lee, Vibration of circular rings with local deviation, *Journal of Applied Mechanics* 61 (1994) 317–322.
[8] H.G. Park, Y.J. Kang, S.H. Kim, Dual mode tuning strategy of a slightly asymmetric ring, *Journal of the Acoustical Society of America* 123 (3) (2008) 1383–1391.
[9] H.G. Park, J.M. Lee, Y.J. Kang, S.H. Kim, A study on the mode pair of a slightly asymmetric circular ring with multiple deviations, *Journal of Sound and Vibration* 310 (2008) 366–380.
[10] M. Ruzzene, A. Fasana, L. Garibaldi, B. Piombo, Natural frequencies and dampings identification using wavelet transform: application to real data, *Mechanical Systems and Signal Processing* 11 (2) (1997) 207–218.
[11] J. Lardies, S. Gouttebroze, Identification of modal parameters using the wavelet transform, *International Journal of Mechanical Sciences* 44 (2002) 2263–2283.
[12] Y.H. Cho, J.M. Lee, S.Y. Park, E.S. Lee, Robust measurement of damping ratios of a railway contact wire using wavelet transforms, *Key Engineering Materials* 321–323 (2006) 1629–1635.
[13] S. Erlicher, P. Argoul, Modal identification of linear non-proportionally damped systems by wavelet transform, *Mechanical Systems and Signal Processing* 21 (2007) 1386–1421.
[14] C. Smith, C.M. Akujuobi, P. Hamory, K. Kloesel, An approach to vibration analysis using wavelets in an application of aircraft health monitoring, *Mechanical Systems and Signal Processing* 21 (2007) 1255–1272.
[15] T. Figarella, M.H. Jansen, Brush wear detection by continuous wavelet transform, *Mechanical Systems and Signal Processing* 21 (2007) 1212–1222.
[16] W.J. Wang, P.D. McFadden, Application of wavelets to gearbox vibration signals for fault detection, *Journal of Sound and Vibration* 192 (2) (1996) 927–939.
[17] J. Slavič, I. Simonovski, M. Boltežar, Damping identification using a continuous wavelet transform: application to real data, *Journal of Sound and Vibration* 262 (2003) 291–307.
[18] T.-P. Le, P. Argoul, Continuous wavelet transform for modal identification using free decay response, *Journal of Sound and Vibration* 277 (2004) 73–100.
[19] S. Mallat, *A Wavelet Tour of Signal Processing*, second ed., Academic Press, New York, 1998.
[20] Y.Y. Kim, E.H. Kim, A new damage detection method based on a wavelet transform, *Proceedings of 18th IMAC*, 2000, pp. 1207–1212.